American Mineralogist, Volume 82, pages 729–739, 1997

# Dehydration dynamics of stilbite using synchrotron X-ray powder diffraction

GIUSEPPE CRUCIANI,[1] GILBERTO ARTIOLI,[2] ALESSANDRO GUALTIERI,[3] KENNY STÅHL,[4] AND JONATHAN C. HANSON[5]

[1]Istituto di Mineralogia, Università di Ferrara, I-44100 Ferrara, Italy
[2]Dipartimento di Scienze della Terra, Università di Milano, I-20133 Milano, Italy
[3]Dipartimento di Scienze della Terra, Università di Modena, I-41100 Modena, Italy
[4]Chemistry Department, Technical University of Denmark, DK-2800 Lyngby, Denmark
[5]Chemistry Department, Brookhaven National Laboratory, Upton, NY 11973, U.S.A.

## ABSTRACT

The continuous structural transformation of the natural zeolite stilbite ($Na_{3.62}K_{0.44}Ba_{0.03}Ca_{6.32}Sr_{0.28}Mg_{0.04}[Fe^{3+}_{0.01}Al_{17.33}Si_{54.64}O_{144}]\cdot 60H_2O$) upon dehydration has been studied using Rietveld structure analysis of temperature-resolved powder diffraction data collected with synchrotron radiation. In the initial stage of heating, the monoclinic *F2/m* stilbite structure (the so-called A phase) behaves as a noncollapsible framework, featuring only a slight framework distortion and a slight cell-volume contraction. At about 420 K, a first-order phase transition occurs changing the symmetry to an orthorhombic *Amma* phase, whose framework is collapsible and shows a large cell-volume contraction with temperature. The cell contraction is related to the process of T-O-T bond breaking and leads to a high-temperature stilbite phase with the same *Amma* space group and a collapsed structure similar to the previously described B phase in stellerite and barrerite. The structural refinement indicates that the dynamics of bond breaking is related to the shift of the Ca cations in the channels to achieve optimal coordination after the release of the $H_2O$ molecules. Refined statistical occupancies of the tetrahedral atoms involved in the bond-breaking process (T1 and T1P) are consistent with a random rupture and re-formation of the T-O-T bonds. This is the first experimental study of the dynamic bond breaking of T-O-T bonds in a framework structure.

## INTRODUCTION

Stilbite ($Na_2Ca_8[Al_{18}Si_{54}O_{144}]\cdot 60H_2O$) is a common zeolite having the same framework topology [STI] of stellerite ($Ca_8[Al_{16}Si_{56}O_{144}]\cdot 56H_2O$) and barrerite ($Na_{16}[Al_{16}Si_{56}O_{144}]\cdot 52H_2O$). The topological symmetry is orthorhombic *Fmmm,* which is also the real symmetry in stellerite (Galli and Alberti 1975a). The real symmetry is orthorhombic *Amma* in barrerite (Galli and Alberti 1975b) and monoclinic *C2/m* in stilbite (Slaughter 1970). In the latter case the non-standard *F2/m* space group is commonly used to facilitate comparison between the related structures.

The thermal behavior of all three stilbite-type minerals has been widely investigated because of their potential use as molecular sieves and catalysts. Early TGA, DTA, and XRD investigations (Aumento 1966; Abbona and Franchini Angela 1969; Simonot-Grange et al. 1970) showed that in stilbite, barrerite, and stellerite one main phase transition occurred at about 420 K leading to a contracted new phase (usually, and hereafter, called B phase for all the three stilbite-type zeolites).

The crystal structures of the B phase in barrerite (Alberti and Vezzalini 1978) and in stellerite (Alberti et al. 1978) have orthorhombic symmetry *Amma.* By analogy the same space group was suggested for the B phase in stilbite. The tetrahedral frameworks of both barrerite B and stellerite B are remarkably distorted and characterized by broken T-O-T bridges (with a fault density of 10% in stellerite B and 56% in barrerite B) and by a configuration with Si,Al tetrahedra inside the channels. This process can be seen as the formation of new partially occupied tetrahedral sites in a face-sharing relationship with the vacant tetrahedra. The occurrence of broken T-O-T bonds has also been described in the contracted B phase of heulandite (Alberti and Vezzalini 1983a). Pearce et al. (1980) and Mortier (1983) observed that both the crystal structures of the dehydrated $NH_4$- and $Na,NH_4$-exchanged forms of stilbite are only slightly distorted and have the same symmetry with respect to the natural form. In the $Na,NH_4$-dehydrated form one T-O-T bridge underwent partial breaking (10% fault density) with the formation of a new tetrahedron inside the secondary building unit (Mortier 1983).

The high-temperature structures of zeolites are often studied by conventional single-crystal diffraction performed at room temperature on crystals previously dehydrated in vacuum at a selected temperature, and subsequently sealed in glass capillaries. Alternatively,

0003–004X/97/0708–0729$05.00

crystals may be treated by flushing with dry $N_2$ maintained at a selected temperature, and then quenched to 100 K for data collection (Armbruster and Gunter 1991). However the latter treatment does not permit discrimination between temperature and vacuum effects on the dehydration process, and it often obscures hysteresis effects from non-equilibrium conditions. Moreover, the mosaicity of the single crystals is drastically increased during the heat treatment, and this severely limits the number of heating cycles the crystal can withstand.

Most of the above problems can be easily overcome by using fast data collection at brilliant synchrotron sources and powder samples instead of single crystals. In-situ synchrotron X-ray powder diffraction is therefore the best suited experimental technique for studying temperature-induced transformation, and the outstanding quality of the powder data collected in this way can be used for full-profile Rietveld structural analysis (Ståhl 1994; Ståhl and Hanson 1995). The aim of the present study is the application of these advanced techniques for the detailed analysis of the structural modifications of stilbite undergoing thermal dehydration.

## Experimental procedure

The stilbite sample is from calcalkaline volcanics at Cape Marargiu near Bosa, Sardinia, Italy. The unit-cell content, $Na_{3.62}K_{0.44}Ba_{0.03}Ca_{6.32}Sr_{0.28}Mg_{0.04}[Fe^{3+}_{0.01}Al_{17.33}Si_{54.64}O_{144}]\cdot 60H_2O$, was determined by an ARL-SEMQ electron probe microanalyzer operating at 15 kV and 20 nA. The electron beam was defocused to approximately 20 μm in diameter to minimize crystal damage. On-line data reduction was based on the Ziebold and Ogilvie (1964) method using Albee and Ray (1970) correction factors. The $H_2O$ content was measured on approximately 10 mg of sample by TG analysis using a Dupont 951 instrument working in air. Chemical analyses were normalized on the basis of 144 O atoms.

## Powder diffraction experiment

The powder spectra were collected at beamline X7B at the National Synchrotron Light Source, Brookhaven National Laboratory, New York, U.S.A. A curved position-sensitive detector covering a range of 120° 2θ (CPS120 by INEL) (Ståhl and Thomasson 1992) was used to record the diffraction patterns. A wavelength of 1.488 Å was selected to gain quantum efficiency of the detector. The count rate was in the range 21 000 to 30 000 counts/s to avoid detector saturation. Single crystals of stilbite with a well-developed platy morphology were ground in an agate mortar. The powder sample was packed in a 0.3 mm diameter Lindemann capillary, open at both ends, and attached to a standard goniometer head. The latter was mounted on the φ axis of the diffractometer and axially spun during data collection in the Debye-Scherrer geometry. Several data sets were recorded intermittently while the specimen was heated in situ. Two complete sets of histograms were collected in the temperature range 315–723 K, using different heating rates. Temperature steps were 6 K for the first data set and 30 K for the second one, each histogram being accumulated for 5 min at constant temperature. The first data set consists of 67 histograms, the second of 16 histograms. Two isothermal experiments were performed at 423 and 450 K by rapid heating of the sample at the selected temperature, and then collecting powder patterns with a time resolution of about 15 s.

The raw counts vs. channel data were calibrated and converted into intensity vs. 2θ-equal-step data according to the procedure of Ståhl and Thomasson (1992). The reliability of the wavelength calculation was checked by measuring the unit cell of quartz and silicon standards. Due to the simultaneous accumulation of the whole angular range of each powder pattern, no incident beam decay correction was necessary.

Further details concerning the beamline optics, the diffractometer set-up, the detector and heater adjustments to reduce additional background, and the data acquisition system, are described elsewhere (Hastings et al. 1983; Ståhl and Hanson 1995 and references therein).

## Rietveld refinement

The structure refinement by Rietveld profile fitting was performed using the GSAS package (Larson and Von Dreele 1994). More than 40 patterns were fit out of the 67 available in the first data set, covering the temperature range 315–723 K. A Simpson's rule integration (Howard 1982) of the pseudo-Voigt function (Thompson et al. 1987) was used to model the peak profile. No asymmetry correction was applied, and a cut-off of 1.0% of peak intensity was used for the Bragg peak calculation limit. Background modeling used a seven-coefficient cosine Fourier series function. The 2θ-zero shift was accurately refined in the first pattern (room temperature) of the data set and constrained to be constant for the remaining ones. One scale factor and the unit-cell parameters were allowed to vary for all histograms. In the final cycles, the refined structural parameters for each data histogram were as following: fractional coordinates for all atoms, occupancy factors for extra-framework cations, the O atoms $H_2O$ (W), partially occupied framework sites (see below), and four isotropic displacement factors (one each for tetrahedral sites, framework O atoms, Ca,Na site, and W atoms). Occupancy factors and isotropic displacement factor coefficients were varied in alternate cycles. Scattering factors for neutral atoms are those listed by Cromer and Waber (1974). The partially occupied sites of the extra-framework cations were modeled by using neutral Ca scattering curves.

The refinements of the A phase of stilbite (in the temperature range 315–416 K) were performed in the pseudo-orthorhombic space group *F2/m*, for ease of comparison with barrerite and stellerite. Starting parameters were taken from Galli (1971) and Quartieri and Vezzalini (1987); the same labeling of atomic sites was also used. Refinements of all coordinates converged successfully for histograms up to 416 K. Refinement of the pattern at 422

**TABLE 1.** Data measurement and refinement parameters for stilbite from Cape Marargiu, Sardinia

| Temperature (K) | 315 | 416 | 441 | 521 |
|---|---|---|---|---|
| Space group | *F2/m** | *F2/m** | *Amma* | *Amma* |
| *a* (Å) | 13.6334(6) | 13.6520(7) | 13.7200(5) | 13.5849(4) |
| *b* (Å) | 18.2443(8) | 18.1575(8) | 17.6808(8) | 17.6213(7) |
| *c* (Å) | 17.8449(9) | 17.790(1) | 17.4461(8) | 17.1148(7) |
| β (°) | 90.320(4) | 90.227(6) | 90 | 90 |
| Cell volume (Å³) | 4438.5(3) | 4409.9(3) | 4232.1(2) | 4097.0(2) |
| $R_p$ (%) | 6.64 | 6.55 | 5.66 | 4.55 |
| $R_{wp}$ (%) | 8.67 | 8.62 | 7.65 | 6.13 |
| $R_{F_{obs}}$ (%) | 10.90 | 10.31 | 16.04 | 11.48 |
| $\chi^2$ | 10.9 | 9.2 | 4.3 | 2.4 |
| No. of variables | 60 | 88 | 74 | 87 |
| No. of observations | 3699 | 3698 | 3710 | 3710 |
| No. of reflections | 1839 | 1829 | 1846 | 1779 |

*Notes:* Composition: $Na_{3.62}K_{0.44}Ba_{0.03}Ca_{6.32}Sr_{0.28}Mg_{0.04}[Fe_{0.01}Al_{17.33}Si_{54.64}O_{144}]\cdot 60H_2O$; Radiation: synchroton X-rays, wavelength = 1.488 Å; Diffraction geometry: Debye-Scherrer. $R_p = \Sigma[Y_{io} - Y_{ic}]/\Sigma Y_{io}$; $R_{wp} = [\Sigma w_i(Y_{io} - Y_{ic})^2/\Sigma w_i Y_{io}^2]^{0.5}$; $R_{F_{obs}} = \Sigma||F_o^2| - |F_c^2||/\Sigma|F_o^2|$; $\chi^2 = \Sigma w_i(Y_{io} - Y_{ic})^2/(N_{obs} - N_{var})$; Estimated standard deviations in parentheses refer to the last digit.

* Non-standard space group for ease of comparison.

K ended with a large $R$ value, and the attempt to refine fractional coordinates for the histogram at 429 K using the model refined for the A phase at 416 K also did not succeed. This was a clear indication that a phase transition had occurred between 416 and 422 K. A preliminary refinement of the unit-cell parameters was performed for the remaining powder data histograms up to 723 K, and, on the basis of the resulting cell values, the histogram at 521 K was tentatively assumed to be the stable collapsed structure of stilbite B phase. The framework atomic coordinates of stellerite B phase (Alberti et al. 1978) were taken as the starting model for the refinement of the stilbite B phase structure; the same labeling of atomic sites was also used. The systematic absence of reflections $hk0$, for $h = 2n + 1$, confirmed the space group to be *Amma*. Extra-framework atomic positions were located and refined by a combination of difference-Fourier maps and least-squares refinement. Electron density maxima corresponding to partially occupied tetrahedral sites were found and refined. Because of the high degree of static disorder, it was possible to locate only part of the original content of the extra-framework cation in both the partially and the fully dehydrated structures. Starting from the structure model of the B phase, i.e., the preliminary refinement on the 521 K histogram, all the histograms in the temperature range 436–700 K, were successfully refined.

The structures refined for stilbite A phase at 416 K and that of stilbite B phase at 436 K were used in a two-phase refinement using the isotherm data collected at 423 K. To obtain the variation of the relative proportions of the two phases with time, only cell parameters and phase-fractions were allowed to vary.

Details of the Rietveld refinements and the full list of refined parameters for stilbite A at 315 K and at 416 K and for stilbite B at 441 K and at 521 K are reported in Tables 1 and 2, respectively. Observed, calculated, and difference powder diffraction patterns are shown in Figure 1. Selected bond distances and angles are given in Table 3. A complete list of refinement parameters and observed and calculated patterns for all histograms are available on request from the corresponding author (G.C.).

## RESULTS

### Unit-cell variation on dehydration

The stepwise dehydration process in stilbite can be monitored by the variation of unit-cell volume (Fig. 2). Only a slight net decrease of the cell volume (−0.64%) is observed below $T$ = 420 K. The sharp contraction (−3.24%) that occurs at 420 K and the further decrease in cell volume (−3.81%) that takes place in the temperature range 430–520 K are both associated to the main phase transition from the monoclinic A phase to the orthorhombic B phase. Between 520 and 700 K only a slight variation (−0.91%) is observed, whereas the final drop in the cell volume (−1.18%), above 700 K, suggests that the stilbite B phase structure starts to collapse. Apart from the absolute temperature scale, which is clearly dependent on the experimental conditions (such as particle size, heating rate, and $H_2O$ pressure), this behavior agrees with the published results of thermal analyses. Reported TGA and DTA spectra of stilbite show two separate endothermal maxima at about 448 and 523 K, corresponding to progressive losses of about 30 and 26 $H_2O$ molecules, respectively; the residual $H_2O$ is released above $T$ = 600 K (Fig. 6.2M of Gottardi and Galli 1985).

Each unit-cell parameter has a unique temperature dependence (Fig. 3). The $b$ cell parameter slightly decreases in the initial stages of the heating process (−0.48%), then it undergoes the largest shortening (−2.61%) in the small $T$ range 420–440 K, while remaining almost unchanged at higher temperature. The small variation of $c$ below 420 K (−0.31%) is similar to that of the $b$ cell parameter, whereas the $c$ contraction at the phase transition temperature is much smaller (−1.62%), and additional shortening takes place gradually between 430 and 520 K (−2.16%). As discussed below, the behavior of the $b$ and $c$ parameters is consistent with the topological constraints imposed on the distortion of the chains of secondary

**TABLE 2a.** Positional parameters, occupancies, and $U_{iso}$ values of stilbite A at 315 and 416 K

| T (K) | Atom | x | y | z | $U_{iso}$ | Occ. |
|---|---|---|---|---|---|---|
| 315 | T1 | 0.3617(8) | 0.3067(7) | 0.1255(6) | 0.023(1) | 1.0 |
| 416 | T1 | 0.3592(9) | 0.3034(6) | 0.1265(7) | 0.023(1) | 1.0 |
| 315 | T2 | 0.1370(7) | 0.3108(7) | 0.1255(6) | 0.023(1) | 1.0 |
| 416 | T2 | 0.1366(9) | 0.3132(7) | 0.1280(7) | 0.023(1) | 1.0 |
| 315 | T3 | −0.0536(7) | 0.0901(4) | 0.2448(7) | 0.023(1) | 1.0 |
| 416 | T3 | −0.0509(8) | 0.0899(5) | 0.2427(8) | 0.023(1) | 1.0 |
| 315 | T4 | −0.1358(6) | 0.3149(5) | 0.2500(7) | 0.023(1) | 1.0 |
| 416 | T4 | −0.1358(7) | 0.3157(6) | 0.2505(8) | 0.023(1) | 1.0 |
| 315 | T5 | 0 | 0.2487(11) | 0 | 0.023(1) | 1.0 |
| 416 | T5 | 0 | 0.2447(11) | 0 | 0.023(1) | 1.0 |
| 315 | O1 | 0.4208(13) | 0.3046(12) | 0.0449(10) | 0.036(1) | 1.0 |
| 416 | O1 | 0.4191(17) | 0.3042(14) | 0.0466(11) | 0.040(1) | 1.0 |
| 315 | O2 | 0.0608(14) | 0.3051(11) | 0.0558(9) | 0.036(1) | 1.0 |
| 416 | O2 | 0.0557(17) | 0.2967(13) | 0.0625(11) | 0.040(1) | 1.0 |
| 315 | O3 | −0.1298(15) | 0.2720(9) | 0.1696(10) | 0.036(1) | 1.0 |
| 416 | O3 | −0.1206(21) | 0.2747(10) | 0.1693(11) | 0.040(1) | 1.0 |
| 315 | O4 | −0.1071(16) | 0.1170(10) | 0.1683(10) | 0.036(1) | 1.0 |
| 416 | O4 | −0.1165(21) | 0.1193(12) | 0.1711(13) | 0.040(1) | 1.0 |
| 315 | O5 | 0.1170(14) | 0.2376(10) | 0.1771(10) | 0.036(1) | 1.0 |
| 416 | O5 | 0.1206(20) | 0.2380(11) | 0.1761(12) | 0.040(1) | 1.0 |
| 315 | O6 | 0.1092(15) | 0.3792(11) | 0.1808(10) | 0.036(1) | 1.0 |
| 416 | O6 | 0.1019(21) | 0.3807(13) | 0.1818(12) | 0.040(1) | 1.0 |
| 315 | O7 | 0.2507(10) | 0.3181(9) | 0.0985(9) | 0.036(1) | 1.0 |
| 416 | O7 | 0.2490(11) | 0.3256(11) | 0.0955(10) | 0.040(1) | 1.0 |
| 315 | O8 | 0.0636(10) | 0.1114(8) | 0.2503(16) | 0.036(1) | 1.0 |
| 416 | O8 | 0.0693(11) | 0.1092(10) | 0.2462(20) | 0.040(1) | 1.0 |
| 315 | O9 | −0.0763(18) | 0 | 0.2394(22) | 0.036(1) | 1.0 |
| 416 | O9 | −0.0644(23) | 0 | 0.2494(33) | 0.040(1) | 1.0 |
| 315 | O10 | −¼ | 0.3451(13) | ¼ | 0.036(1) | 1.0 |
| 416 | O10 | −¼ | 0.3487(16) | ¼ | 0.040(1) | 1.0 |
| 315 | Ca | 0.2373(12) | 0 | 0.0433(7) | 0.092(1) | 0.99(2) |
| 416 | Ca | 0.2440(28) | 0 | 0.0387(14) | 0.094(1) | 0.62(3) |
| 315 | Na | 0.4736(31) | 0.0563(34) | 0.027(4) | 0.092(1) | 0.22(3) |
| 416 | Na | 0.334(7) | 0.122(4) | 0.083(4) | 0.094(1) | 0.36(4) |
| 315 | W1 | 0.085(4) | 0.089(3) | 0.060(3) | 0.112(3) | 0.41(2) |
| 416 | W1 | 0.110(7) | 0.074(6) | 0.078(5) | 0.120(5) | 0.36(4) |
| 315 | W2 | 0.288(4) | 0.130(1) | 0.060(2) | 0.112(3) | 1.00(2) |
| 416 | W2 | 0.250(7) | 0.139(3) | 0.059(3) | 0.120(5) | 0.64(5) |
| 315 | W3 | 0.183(2) | 0 | 0.190(1) | 0.112(3) | 1.00(4) |
| 416 | W3 | 0.194(5) | 0 | 0.198(3) | 0.120(5) | 0.88(8) |
| 315 | W4 | 0.404(2) | 0 | 0.109(2) | 0.112(3) | 1.00(3) |
| 416 | W4 | 0.417(5) | 0 | 0.072(4) | 0.120(5) | 0.97(7) |
| 315 | W5 | 0.383(4) | ½ | 0.075(2) | 0.112(3) | 0.66(4) |
| 416 | W5 | 0.383(9) | ½ | 0.082(5) | 0.120(5) | 0.58(8) |
| 315 | W6 | 0.138(2) | ½ | 0.046(2) | 0.112(3) | 0.87(5) |
| 416 | W6 | 0.110(5) | ½ | 0.051(4) | 0.120(5) | 0.98(10) |
| 315 | W8 | 0.227(3) | 0 | −0.094(1) | 0.112(3) | 0.73(3) |
| 416 | W8 | 0.214(7) | 0 | −0.100(3) | 0.120(5) | 0.70(7) |

*Note:* Estimated standard deviations in parentheses refer to the last digit.

building units parallel to the [001] direction. Conversely, the *a* cell parameter slightly increases below 420 K (+0.14%), it exhibits a marked elongation at the phase transition (+0.5%), and it shortens by −0.99% in the temperature range 450–550 K. It is noteworthy that a similar lengthening was also observed in stellerite B by Alberti et al. (1978). This behavior may be qualitatively explained by the decreased number of hydrogen bonds between the $H_2O$ molecules and the framework O atoms. The angle β in the A phase gets progressively closer to 90° as the temperature approaches the transition temperature (Fig. 3, inset), in agreement with the framework's tendency to approach orthorhombic symmetry.

### Structural distortion on dehydration

The framework of natural stilbite (A phase, Fig. 4a) is formed by 4 − 4 = 1 secondary building units (SBU) (Meier and Olson 1978), which are connected by tetrahedral-vertex sharing to form chains parallel to the *c* direction. In the stilbite A phase the T5-T5 vector representing one SBU is nearly parallel to the axis of the chain. The chains are linked laterally through the T3-O9-T3 bridges. The resulting sheets parallel to (010) are joined by O bridges between the T4, T2, and T1 tetrahedra creating a two-dimensional system of intersecting channels, defined by ten- and eight-membered tetrahedral rings, parallel to [100] and to [001], respectively. The Ca atoms are located at the intersection of the two channel systems and are completely surrounded by $H_2O$ molecules. This is a rather unusual feature for extra-framework Ca cations in zeolites (Fig. 5a). The Na atoms are coordinated by $H_2O$ molecules and framework O atoms. In the monoclinic stilbite A phase the ten-membered-ring delimited channels are all symmetrically equivalent.

**TABLE 2b.** Positional parameters, occupancies, and $U_{iso}$ values of stilbite B at 441 and 521 K

| T (K) | Atom | x | y | z | $U_{iso}$ | Occ. |
|---|---|---|---|---|---|---|
| 441 | T1 | 0.1383(8) | 0.3289(6) | 0.1327(7) | 0.036(1) | 1.00(1) |
| 521 | T1 | 0.1421(9) | 0.3381(8) | 0.1329(7) | 0.036(1) | 0.64(1) |
| 441 | T1D | — | — | — | — | — |
| 521 | T1D | 0.1412(10) | 0.4124(8) | 0.1106(9) | 0.036(1) | 0.36(1) |
| 441 | T1P | 0.1372(7) | 0.2897(5) | 0.3782(6) | 0.036(1) | 1.00(1) |
| 521 | T1P | 0.1394(7) | 0.2756(6) | 0.3761(6) | 0.036(1) | 0.97(1) |
| 441 | T1PD | — | — | — | — | — |
| 521 | T1PD | 0.1505(11) | 0.3244(10) | 0.4364(12) | 0.036(1) | 0.01(1) |
| 441 | T3 | 0.0493(8) | 0.4084(6) | 0.2760(6) | 0.036(1) | 1.0 |
| 521 | T3 | 0.0540(7) | 0.4125(5) | 0.2866(7) | 0.036(1) | 1.0 |
| 441 | T4 | 0.1359(8) | 0.1864(6) | 0.2336(6) | 0.036(1) | 1.0 |
| 521 | T4 | 0.1370(7) | 0.1756(6) | 0.2234(7) | 0.036(1) | 1.0 |
| 441 | T5 | 0 | 0.2935(7) | 0 | 0.036(1) | 1.0 |
| 521 | T5 | 0 | 0.3044(8) | 0 | 0.036(1) | 1.0 |
| 441 | O1 | 0.0673(16) | 0.3468(9) | 0.0577(12) | 0.052(1) | 1.0 |
| 521 | O1 | 0.0693(12) | 0.3568(9) | 0.0586(10) | 0.052(1) | 1.0 |
| 441 | O1P | 0.0666(13) | 0.2668(9) | 0.4520(11) | 0.052(1) | 1.0 |
| 521 | O1P | 0.0777(12) | 0.2514(9) | 0.4542(9) | 0.052(1) | 1.0 |
| 441 | O3 | 0.1212(20) | 0.2417(9) | 0.1601(11) | 0.052(1) | 1.0 |
| 521 | O3 | 0.1339(14) | 0.2473(8) | 0.1595(11) | 0.052(1) | 1.00(2) |
| 441 | O3D | — | — | — | — | — |
| 521 | O3D | −0.107(4) | 0 | 0.412(4) | 0.052(1) | 0.57(4) |
| 441 | O3P | 0.1232(19) | 0.2143(11) | 0.3225(9) | 0.052(1) | 1.00(1) |
| 521 | O3P | 0.1266(14) | 0.2081(9) | 0.3123(8) | 0.052(1) | 1.00(2) |
| 441 | O4 | 0.1015(16) | 0.3888(11) | 0.1955(7) | 0.052(1) | 1.0 |
| 521 | O4 | 0.0996(13) | 0.3971(11) | 0.1992(9) | 0.052(1) | 1.0 |
| 441 | O4P | 0.1250(15) | 0.3740(9) | 0.3375(9) | 0.052(1) | 1.0 |
| 521 | O4P | 0.1021(13) | 0.3635(8) | 0.3577(10) | 0.052(1) | 1.0 |
| 441 | O7 | ¼ | 0.3635(12) | 0.1153(23) | 0.052(1) | 1.0 |
| 521 | O7 | ¼ | 0.3698(14) | 0.1007(16) | 0.052(1) | 1.0 |
| 441 | O7P | ¼ | 0.2783(12) | 0.4051(17) | 0.052(1) | 1.0 |
| 521 | O7P | ¼ | 0.2749(17) | 0.4150(15) | 0.052(1) | 1.0 |
| 441 | O8 | 0.0652(11) | 0.1162(10) | 0.2104(14) | 0.052(1) | 1.0 |
| 521 | O8 | 0.0668(10) | 0.0996(9) | 0.2182(13) | 0.052(1) | 1.0 |
| 441 | O9 | 0.0627(24) | ½ | 0.2979(18) | 0.052(1) | 1.0 |
| 521 | O9 | 0.0856(19) | ½ | 0.3101(16) | 0.052(1) | 1.0 |
| 441 | O10 | ¼ | 0.1579(16) | 0.2265(18) | 0.052(1) | 1.0 |
| 521 | O10 | ¼ | 0.1389(13) | 0.2234(16) | 0.052(1) | 1.0 |
| 441 | C1 | ¼ | 0.315(5) | 0.082(5) | 0.078(1) | 0.18(2) |
| 521 | C1 | ¼ | 0.2468(22) | 0.0494(23) | 0.078(1) | 0.31(1) |
| 441 | C2 | 0.205(7) | 0 | 0.251(6) | 0.078(1) | 0.12(1) |
| 521 | C2 | 0.191(5) | 0 | 0.230(5) | 0.078(1) | 0.13(1) |
| 441 | C4 | ¼ | ½ | 0.1119(33) | 0.078(1) | 0.33(2) |
| 521 | C4 | ¼ | ½ | 0.1917(24) | 0.078(1) | 0.38(2) |
| 441 | C5 | ¼ | ½ | 0.422(4) | 0.078(1) | 0.28(2) |
| 521 | C5 | ¼ | ½ | 0.479(8) | 0.078(1) | 0.11(2) |
| 441 | W1 | 0.142(5) | 0 | 0.389(4) | 0.090(4) | 0.49(4) |
| 521 | W1 | 0.187(5) | 0 | 0.390(5) | 0.090(4) | 0.34(3) |
| 441 | W2 | 0.0443(25) | 0 | 0.5851(18) | 0.090(4) | 1.06(4) |
| 521 | W2 | 0.186(17) | 0 | 0.529(15) | 0.090(4) | 0.13(4) |
| 441 | W3 | 0.107(4) | 0 | −0.052(4) | 0.090(4) | 0.58(4) |
| 521 | W3 | 0.053(7) | 0 | 0.029(7) | 0.090(4) | 0.26(3) |

*Note:* Estimated standard deviations in parentheses refer to the last digit. Dashes mean vacant.

**Below the phase transition.** The structural modifications in the initial stages of the dehydration process may be generally regarded as the tendency of the structure to adopt an orthorhombic symmetry. This is obtained by the progressive shift of the Ca atom along the [100] direction toward the orthorhombic pseudo-mirror plane at $x = ¼$ (Fig. 6), which is likely restored as a consequence of the decreasing interactions with the Na atoms. This interaction was previously assumed to be the primary cause for the symmetry lowering in natural stilbite (Galli and Alberti 1975b).

The slight distortion of the framework is related to the rotation of the tetrahedral 4 − 4 = 1 SBU (designated by the angle α, Fig. 4). Alternating SBUs in the same chain rotate in opposite directions in the (100) plane, the T5-O1-T1 and T5-O2-T2 bridges acting as hinges (Fig. 4b). Simultaneously, adjacent tetrahedral units along [100] belonging to different chains also counter-rotate with respect to each other. In other words, two adjacent T5 positions along [100] at (0,*y*,0) and at (½,*y*,0) are related by an inversion center at (¼,¼,0) in the *F2/m* space group. The coupling of both counter-rotations provides a planar relaxation of the (010) plane containing the SBUs chains, which make the O9 atoms, bridging the units along [010], shift toward the pseudo-mirror plane at $z = ¼$. As α reaches a value of about 1.2°, the shift of the O9 atom makes the T3-O9-T3 angle approach 180°, which in turn allows more regular projection of the ten-membered-ring channels.

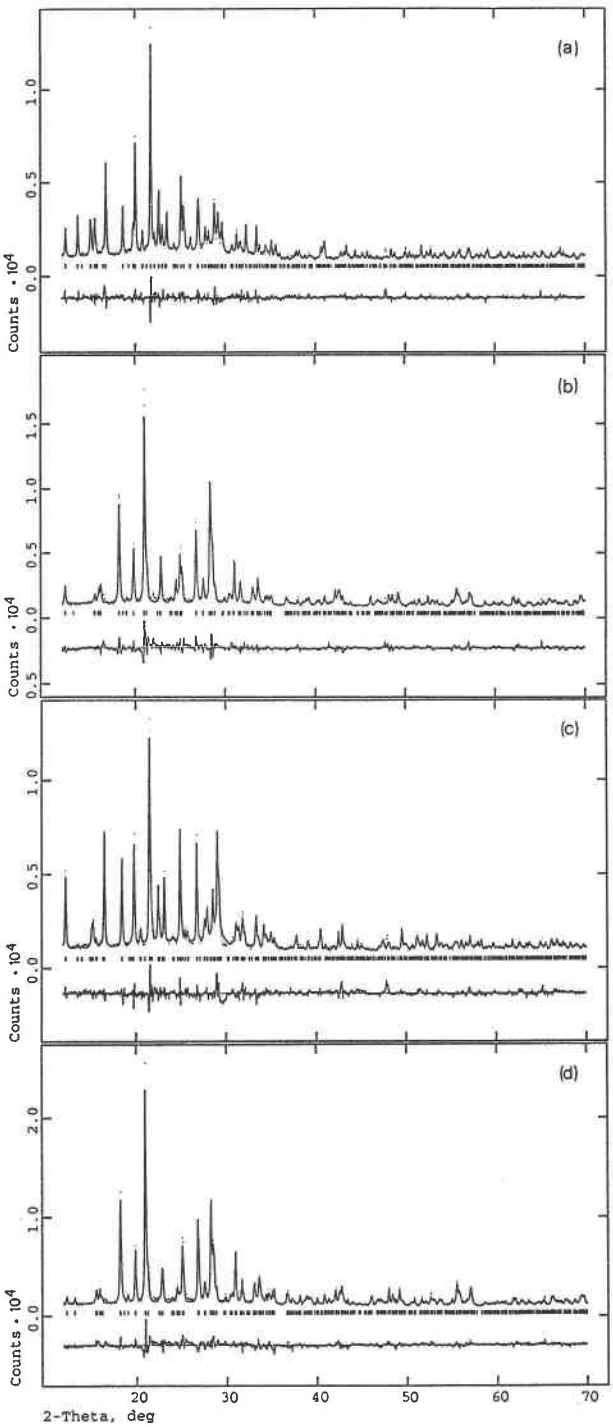


**FIGURE 1.** Observed (dotted line) and calculated (continuous line) diffraction patterns, and final difference curve from Rietveld refinements of stilbite at (**a**) 315 K, (**b**) 416 K, (**c**) 441 K, and (**d**) 521 K.

**TABLE 3.** T-O distances and M-O distances* (Å) for channel cations

| Stilbite A | | | Stilbite B | | |
|---|---|---|---|---|---|
| | 315 K | 416 K | | 441 K | 521 K |
| T1-O1 | 1.65(1) | 1.64(1) | T1-O1 | 1.66(1) | 1.645(8) |
| T1-O3 | 1.64(1) | 1.63(1) | T1-O3 | 1.63(1) | 1.668(8) |
| T1-O4 | 1.64(1) | 1.64(1) | T1-O4 | 1.61(1) | 1.643(8) |
| T1-O7 | 1.60(1) | 1.65(1) | T1-O7 | 1.68(1) | 1.662(8) |
| | | | T1D-O1 | | 1.645(9) |
| | | | T1D-O4 | | 1.641(9) |
| | | | T1D-O7 | | 1.667(9) |
| | | | T1D-O3D | | 1.658(9) |
| | | | T1PD-O1 | | 1.65(1) |
| | | | T1PD-O4 | | 1.64(1) |
| | | | T1PD-O7 | | 1.66(1) |
| | | | T1PD-O3PD† | | — |
| T2-O2 | 1.62(1) | 1.63(1) | T1P-O1P | 1.66(1) | 1.634(8) |
| T2-O5 | 1.64(1) | 1.63(1) | T1P-O3P | 1.66(1) | 1.624(8) |
| T2-O6 | 1.64(1) | 1.63(1) | T1P-O4P | 1.66(1) | 1.660(8) |
| T2-O7 | 1.63(1) | 1.66(1) | T1P-O7P | 1.63(1) | 1.643(8) |
| T3-O4 | 1.62(1) | 1.64(1) | T3-O4 | 1.61(1) | 1.643(8) |
| T3-O6 | 1.63(1) | 1.61(1) | T3-O4P | 1.61(1) | 1.628(8) |
| T3-O8 | 1.65(1) | 1.68(1) | T3-O8 | 1.65(1) | 1.657(8) |
| T3-O9 | 1.674(8) | 1.648(9) | T3-O9 | 1.679(9) | 1.650(7) |
| T4-O3 | 1.64(1) | 1.64(1) | T4-O3 | 1.63(1) | 1.672(8) |
| T4-O5 | 1.64(1) | 1.64(1) | T4-O3P | 1.64(1) | 1.632(8) |
| T4-O8 | 1.67(1) | 1.64(1) | T4-O8 | 1.63(1) | 1.647(8) |
| T4-O10 | 1.651(8) | 1.671(9) | T4-O10 | 1.649(9) | 1.665(7) |
| T5-O1 × 2 | 1.662(8) | 1.644(8) | T5-O1 × 2 | 1.660(7) | 1.656(6) |
| T5-O2 × 2 | 1.651(8) | 1.644(8) | T5-O1P × 2 | 1.634(7) | 1.643(6) |
| \|α\|‡ | 0.3(2) | 1.2(4) | T5-O1P × 2 | 9.9(3) | 12.6(2) |
| Ca-W1 × 2 | 2.66(1) | 2.38(9) | C4-O4 × 4 | | 2.73(2) |
| Ca-W2 × 2 | 2.487(5) | 2.56(5) | C4-O7 × 2 | 2.41(2) | 2.77(3) |
| Ca-W3 | 2.72(1) | 2.92(5) | C4-O9 × 2 | | 3.02(4) |
| Ca-W4 | 2.55(1) | 2.43(7) | C4-O3D × 2 | | 2.63(5) |
| Ca-W5 | 2.67(1) | 2.75(9) | C4-W2 × 2 | 2.86(3) | 2.93(2) |
| Ca-W6 | 2.33(1) | 2.57(7) | C1-O1 × 2 | 2.60(3) | |
| Ca-W8 | 2.46(1) | 2.50(6) | C1-O3 × 2 | 2.58(6) | 2.46(3) |
| Na-O2 | 2.96(6) | | C1-O7 | | 2.34(4) |
| Na-O2 | 2.84(7) | | C1-O7P | | 2.33(4) |
| Na-O3 | | 2.50(7) | C2-O8 × 2 | 2.89(6) | 2.44(5) |
| Na-W2 | 2.93(4) | | C2-O10 × 2 | 2.89(4) | 2.58(3) |
| Na-W4 | 2.04(6) | 2.50(9) | C2-W1 | 2.56(9) | |
| Na-W6 | 2.49(3) | | C5-W3 | 2.01(6) | 2.82(9) |
| Na-W6 | 2.25(7) | | | | |

*Notes:* Estimated standard deviations in parentheses refer to the last digit.

* M-O distances less than 3.1 Å.

† The position of the O3PD atom was not clearly located on the Fourier map.

‡ |α| (°): absolute value of rotation of the 4 − 4 = 1 units around their center of gravity in the (100) plane calculated as $\alpha = \cot [y_{T5} - 0.25)b/(0.25c \sin \beta)]$.

The refinement of the site occupancy factors of the $H_2O$ molecules at 416 K indicates a general decrease of the total $H_2O$ content, though none of the $H_2O$ molecule sites seems to be completely vacant. The refinement at 422 K yielded a zero occupancy of the W3 site, within errors, suggesting that this $H_2O$ site is the first to be emptied at the onset of the phase transition. The decrease in the Ca site scattering density is consistent with the diffusion of the Na cations out of this site.

**Near the phase transition.** The structure of the stilbite phase appearing at 420 K was refined in the orthorhombic *Amma* space group. The variation of the phase fractions of the stilbite A phase and B phase vs. time, as refined using the isotherm data at 423 K, shows that the disap-

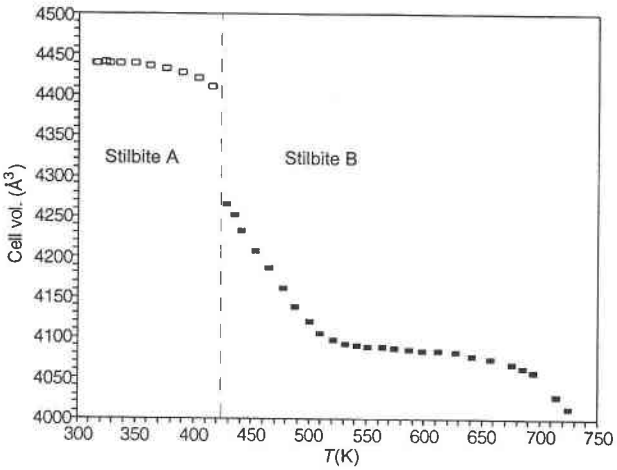


FIGURE 2. Plot of unit-cell volume vs. temperature. Open and solid symbols are for stilbite A and stilbite B, respectively.

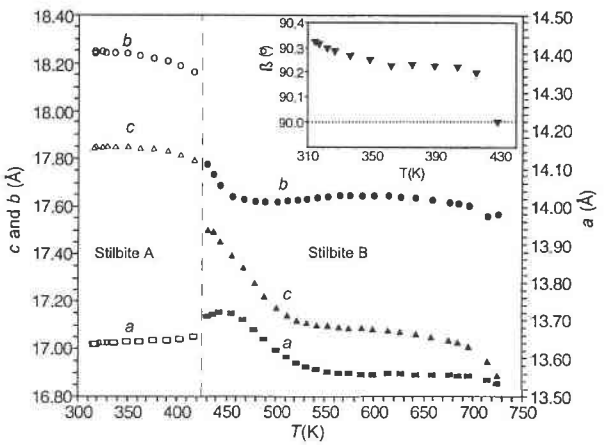


FIGURE 3. Plot of unit-cell parameters vs. temperature. Open and solid symbols as in Figure 2: Circles are for *b*, triangles for *c*, and boxes for *a* cell parameters. The scale for *a* is about 60% larger than that for *c* and *b*. The inset shows the variation of β in stilbite A.

pearance of monoclinic phase (A phase) and the growth of the orthorhombic phase (B phase) are instantaneous.

In the space group *Amma* the chains of SBU passing through T5 at *(0,y,0)* and at *(½,y,0)* become symmetrically related by a mirror plane at $x = ¼$. This implies that in the framework of the orthorhombic B phase, adjacent chains along [100] rotate in the same direction (Fig. 4c). This mechanism is responsible for the large increase of chain rotation in the (100) plane at 420 K (Fig. 7), and it is the cause of the framework distortion and the cell-volume contraction. The channel system in stilbite A phase is formed by only one type of ten-membered-ring channel, whereas in stilbite B phase there are two symmetrically independent channel types characterized by a differently elongated cross-section and by different composition and distribution of extra-framework species.

In the temperature range 436–520 K the crystal structure of the B phase undergoes continuous changes. Most of the $H_2O$ molecules coordinated to the Ca,Na cations in the C4 position are expelled, and the cations are then forced to move closer to the framework O atoms by a shift along the [001] direction (cf. Fig. 6). During this stage the movements of the Ca cations are intimately related to the amount of tetrahedral chain rotation and to the shortening of the *c* cell parameter (cf. Fig. 6, Fig. 7, and Fig. 3).

The structure refinement at 441 K (Fig. 4c) shows that the O7 atom is the only framework O within bonding distance to the C4 site (cf. Table 3). A possible effect of the C4 atom migration along [001] is to pull the O7 atom, causing a tilting of the T1 tetrahedron. The strong stretching effect exerted on the T1-O3-T4 bridging bond explains the appearance, at about 465 K, of small fractions of T1-O3-T4 broken bonds (Fig. 8). The breaking of T1-O3 bonds is also associated with a sudden jump of the C4 atom displacement along [001] (cf. Fig. 6). Meanwhile a small counter-tilting of the 4 − 4 = 1 units around the T5-T5 axis occurs.

**Above the phase transition.** Above 520 K and up to 700 K the framework topology undergoes only very minor geometrical changes. The dehydrated stilbite B structure, which is stable in this range, is characterized by the occurrence of T-O-T broken bonds. Most important is the breaking of T1-O3-T4 bonds and, less significant, of T1P-O3P-T4 bonds. The dynamics of T-O-T bond change might be described by the migration of the tetrahedral T1 (and T1P) cations inside the channels, and by the formation of partially occupied tetrahedral sites labeled T1D (and T1PD) (Fig. 4d). Each T1D tetrahedron has three vertices in common with T1, so that they represent a pair of face-sharing tetrahedra (Alberti and Vezzalini 1983b). The fourth vertex is the O3D position within the channel. The T1D, T1PD, and O3D sites were clearly recognized on the difference-Fourier map, whereas the O3PD position was not clearly located. The refined occupancy of the tetrahedral T1D site reaches a maximum of about 48% above 560 K (Fig. 8), and the slight decrease in the range 560–600 K is due to correlation with the site displacement parameters. The occupancy of the O3D site in the same temperature range is close to 77%, and this seems to indicate that the two symmetry related T1D tetrahedra can be independently occupied, as discussed below. Also the breaking of T4-O3P-T1P bonds and the formation of new T1PD sites seems to increase above 600 K. Refined electron density and nearest-neighbor bond lengths suggest that Ca atoms are preferentially located at the C4 site (cf. Fig. 5b).

At this stage most of the $H_2O$ molecules have been released and the $H_2O$ vapor likely removed throughout the open-ended capillary. Nevertheless, one might suggest that the steam, trapped into the zeolite pores, could be responsible for a partial dealumination of the zeolite framework leading to the formation of extra-framework Al species similar to what has been observed by several

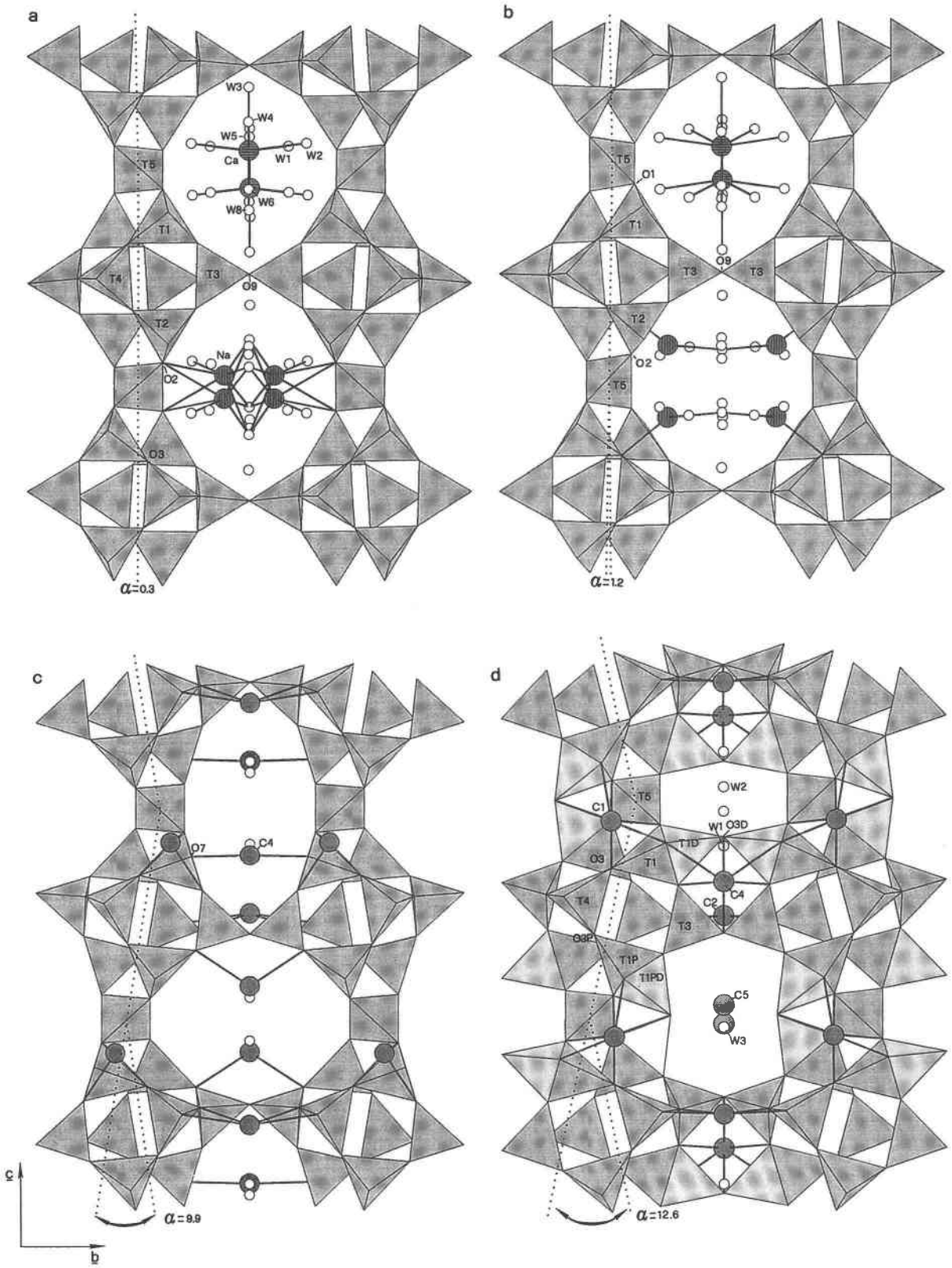
a
W3
W4
W5
Ca
W1
W2
T5
W6
W8
T1
T4
T3
O9
T2
Na
O2
O3
α=0.3
b
T5
O1
T1
O9
T3
T3
T2
O2
T5
α=1.2
c
O7
C4
α=9.9
c
b
d
W2
C1
T5
W1 O3D
T1D
O3
T1
T4
C2
C4
T3
O3P
T1P
T1PD
C5
W3
α=12.6

authors (Parise et al. 1984, and references therein). The refinements and difference-Fourier maps for stilbite at high temperature show no indications for the presence of extra-framework Al species, suggesting that removal of Al from the zeolite framework, if any, is negligible in stilbite B. This is not surprising if we compare our experimental conditions to those used by Parise et al. (1984) to obtain dealuminated Linde Y-zeolite samples. Their samples were treated for 6 h at 823 K with $NH_3$ and steam and gaseous $SiCl_4$, and dehydrated under vacuum before the data collection.

## Discussion

The thermal behavior of the cell parameters in stilbite can be compared with those of stellerite and barrerite listed in Table 1 of Alberti et al. (1978). The measured cell-volume contraction in the dehydrated B phase (−7.7%) is considerably smaller than the one reported for the B phase in stellerite (−12.4%) and in barrerite (−15.7%). The difference is related to the smaller degree of framework distortion observed in stilbite ($\alpha$ = 12.6°), as measured by the structural chain rotation, with respect to barrerite ($\alpha$ = 16.1°) and stellerite ($\alpha$ = 16.4°).

To follow the dehydration behavior of stilbite it is helpful to refer to the descriptions introduced by Alberti and Vezzalini (1983b) and by Baur (1992). Alberti and Vezzalini (1983b) classified the possible topological changes in zeolites upon heating using three processes: (1) reversible dehydration with little or no modifications of the framework and in cell volume; (2) reversible dehydration accompanied by a large distortion of the framework and significant decrease in cell volume; and (3) partially irreversible dehydration accompanied by breaking of T-O-T bonds. According to Baur (1992) the presence of anti-rotating hinges in flexible zeolite structures provides them with a self-limiting mechanism to distortion and these frameworks may be called 'noncollapsible.' On the contrary, the presence of co-rotating hinges in 'collapsible' frameworks enhances the distortion of the structure. From the present data, it is evident that the stilbite framework is noncollapsible in the initial stages of dehydration, featuring just a small framework distortion and a contraction of the cell volume (the first type noted by Alberti and Vezzalini). At the phase transition the framework starts to behave as collapsible, featuring a large distortion even if the major change in cell volume does not involve any breaking of T-O-T bonds (the second type of Alberti and Vezzalini). We suggest that the change in the structure response to temperature can be induced by purely geometrical constraints related to the counter-rotation of the

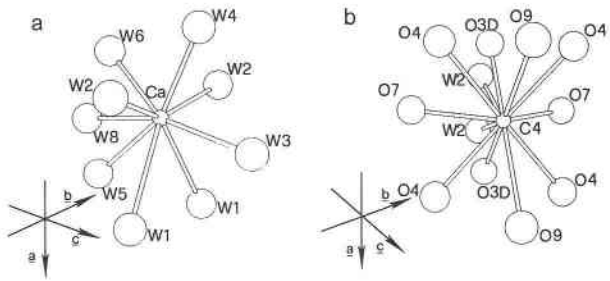


**Figure 5.** Change of the Ca atom coordination during dehydration. (**a**) Ca-$H_2O$ molecule coordination (distances < 2.75 Å) in stilbite A at 315 K; (**b**) C4-framework O atoms and $H_2O$ molecule coordination (distances < 3.10 Å) in stilbite B at 521 K.

SBU chains in monoclinic stilbite. As discussed above, the counter-rotation implies opposite migration of the O9 atom laterally linking the SBU chains atoms toward the (001) pseudo-mirror plane, and leads to values of the T3-O9-T3 angle of very close to 180°. In the topological *Fmmm* symmetry, the T3-O9-T3 bridge lies on the (001) mirror plane. Apparently, this arrangement may act as a geometrical limitation to further counter-rotation of the SBU chains, leading to a change of the distortion mechanism.

Above 470 K the high-temperature phase of stilbite shows evidence of T–O–T bond breaking (the third type of Alberti and Vezzalini), and above 560 K the B phase structure exhibits the highest occupancies of the new T1D and O3D sites. If pairs of mirror-plane–related T1D tetrahedra are occupied at the same time, they form a T1D-O3D-T1D bridge across the boat-shaped ten-membered-ring channels (Fig. 4d). However, the occupancy refined for the O3D site (73%) is very close to the one expected on the basis of a purely statistical occupancy of the two tetrahedra. This is also in agreement with the interpretation of the barrerite behavior, where the presence of OH groups indicates the occurrence of non-shared new O sites (Alberti et al. 1983). It is noteworthy that in the stilbite B phase the statistical occurrence of T1D-O3D-T1D bridges implies the formation of new cages delimited by four-, five-, and six-membered rings of tetrahedra around the C4 extraframework cations (Fig. 5b). The enhanced O mobility associated with the mechanism of tetrahedral bond breaking and formation, occurring at a temperature considerably higher than that of the phase transition, could be the key to understanding the observations of Feng and Savin (1993) about the O isotope exchange process between framework and channel $H_2O$ during the thermal dehydration of stilbite. They found

←

**Figure 4.** Projections along [100] of refined structures for low- and high-temperature stilbite as follows: (**a**) stilbite A phase at 315 K. For clarity, Ca and Na atoms, although coexisting in the same ten-membered-ring channels, are displayed separately in the upper and lower cavities, respectively. Dotted line shows the nearly straight geometry of 4 − 4 = 1 tetrahedral units chains; (**b**) stilbite A at 416 K, same as above with a slighter greater $\alpha$ value; (**c**) stilbite B phase at 441 K. Dotted lines show the counter-rotation of adjacent units in the (100) plane; (**d**) stilbite B at 521 K. The occurrence of newly formed partially occupied tetrahedral sites T1D and T1PD are displayed (light gray).

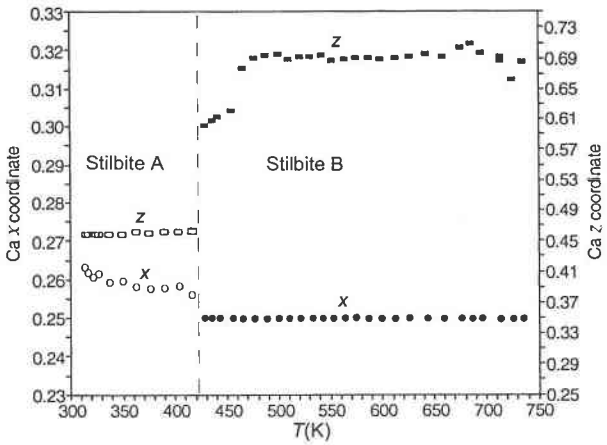


FIGURE 6. Variation of $x$ (circles) and $z$ (boxes) fractional coordinates of the Ca site at ($\frac{1}{2} - x,0,\frac{1}{2} - z$) and at ($\frac{1}{2} - x,\frac{1}{2} + y,\frac{1}{2} + z$) in stilbite A and B, respectively, vs. temperature. Open and solid symbols as in Figure 2.

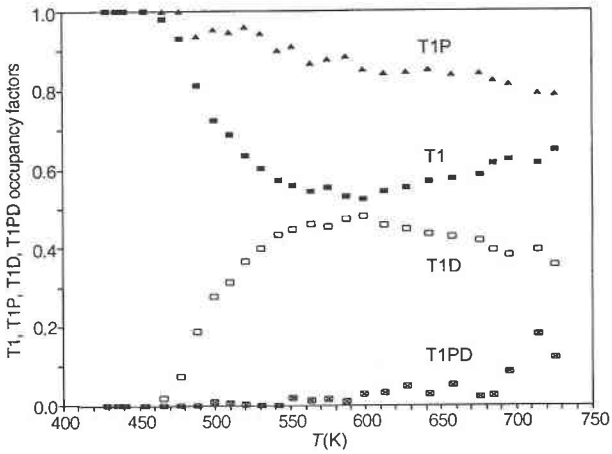


FIGURE 8. Refined occupancies of face-sharing tetrahedral sites vs. temperature above 400 K: T1 (solid boxes), T1D (open boxes), T1P (triangles), and T1PD (boxes with cross).

that the maximum rate of isotope exchange was not related to the A to B phase transition, but noticeably shifted at higher temperature.

The structure refinements show the tendency of the Ca cations to achieve a more stable coordination by increasing the number of Ca-framework O atom bonds. This confirms that the displacement of extra-framework cations may be regarded as the driving force for framework distortion and collapse of dehydrated stilbite-type structures (Alberti and Vezzalini 1983b). The refined atomic density in the C4 position is close to the corresponding site in barrerite B (C4 site, Alberti and Vezzalini 1978), in stellerite B (C4 site, Alberti et al. 1978), in dehydrated $NH_4$ (site 1, Pearce et al. 1980), and in Na-$NH_4$ exchanged forms of stilbite (site 3, Mortier 1982). In all the above structures the position is close to (¼,½,0.21) in the orthorhombic setting, and it exhibits the highest electron density among the extra-framework positions, whether it is occupied by extra-framework cations or by $H_2O$ molecules. It might therefore be tentatively argued that this position is energetically favored in the cavity of the collapsed stilbite-type structures, although in the different structures the radius and electrostatic potential of the guest atom controls the local distortion of the cage.

The B phase structure characterized by a high density of broken T-O-T bonds is stabilized above 520 K, and the structure present in the 420–520 K temperature range can be regarded as a transient orthorhombic phase, possibly related to the 'orthorhombic intermediate metastilbite' of Simonot-Grange et al. (1970), which was interpreted to be due to the loss of six $H_2O$ molecules, as opposed to 'metastilbite' (corresponding to the B phase), characterized by the loss of eight $H_2O$ molecules.

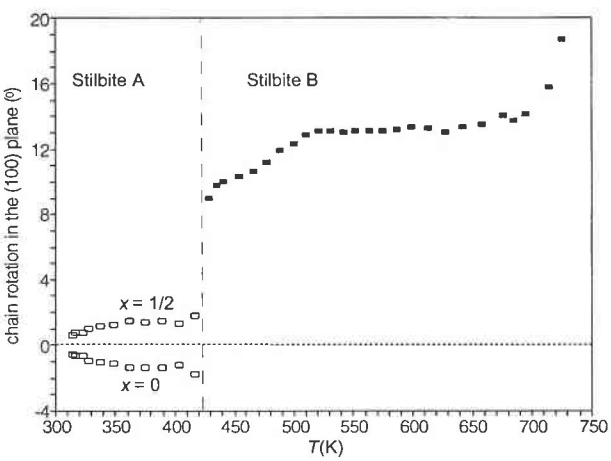


FIGURE 7. Rotation of 4 − 4 = 1 unit chains in the (100) plane vs. temperature. The double trend in stilbite A refers to chains at $x = 0$ and $x = \frac{1}{2}$.

## ACKNOWLEDGMENTS

This work, carried out at Brookhaven National Laboratory, was supported under contract DE-AC02-76CH00016 with the U.S. DOE by its Division of Chemical Sciences, Office of Basic and Energy Sciences, by the Italian CNR and MURST, and by the Swedish NFR. Thanks are due to G. Vezzalini for making the stilbite sample available and for performing the chemical analysis at the electron microprobe facility at the Dipartimento di Scienze della Terra, University of Modena. We also wish to thank those whose critical reviews improved the manuscript: A. Alberti for the helpful discussion, M.E. Gunter for the very thorough and constructive suggestions, and J.B. Higgins for the comments.

## REFERENCES CITED

Abbona, F. and Franchini Angela, M. (1969) Sulla disidratazione della stilbite. Atti dell' Accademia delle Scienze di Torino, 104, 309–321.

Albee, A.L. and Ray, L. (1970) Correction factors for electron-probe microanalysis of silicates, oxides, carbonates, phosphates and sulfates. Analytical Chemistry, 42, 1408–1414.

Alberti, A. and Vezzalini, G. (1978) Crystal structure of heat-collapsed phases of barrerite. In L.B. Sand, and F.A. Mumpton, Eds., Natural Zeolites, p. 85–98. Pergamon Press, New Jersey.

——— (1983a) The thermal behaviour of heulandites: a structural study of the dehydration of Nadap heulandite. Tschermaks mineralogische und petrographische Mitteilungen, 31, 259–270.

——— (1983b) Topological changes in dehydrated zeolites: Breaking of T-O-T bridges: In D. Olson, and A. Bisio, Eds., Proceedings Sixth International Zeolite Conference, Reno, p. 834–841, Butterworths, Guilford, U.K.

Alberti, A., Rinaldi R., and Vezzalini G. (1978) Dynamics of dehydration in stilbite-type structures; stellerite phase B. Physics and Chemistry of Minerals, 68, 880–899.

Alberti, A., Cariati, F., Erre, L., Piu, P., and Vezzalini, G. (1983) Spectroscopic investigation on the presence of OH in natural barrerite and its collapsed phases. Physics and Chemistry of Minerals, 9, 189–191.

Armbruster, T. and Gunter, M.E. (1991) Stepwise dehydration of heulandite-clinoptilolite from Succor Creek, Oregon, U.S.A.: A single-crystal X-ray study at 100 K. American Mineralogist, 76, 1872–1883.

Aumento, F. (1966) Thermal transformations of stilbite. Canadian Journal of Earth Science, 3, 351–366.

Baur, W. H. (1992) Self-limiting distortion by antirotating hinges is the principle of flexible but noncollapsible frameworks. Journal of Solid State Chemistry 97, 243–247.

Cromer, D. T. and Waber, J.R. (1974) Atomic scattering factors for X-rays. In: International Tables for X-Rays Crystallography, Vol. IV, Section 2.2, p. 99–101. The Kynoch Press: Birmingham, U.K.

Feng, X. and Savin, S.M. (1993) Oxygen isotope studies of zeolites-Stilbite, analcime, heulandite, and clinoptilolite: II. Kinetics and mechanisms of isotopic exchange between zeolites and water vapour. Geochimica et Cosmochimica Acta, 57, 4219–4238.

Galli, E. (1971) Refinement of the crystal structure of stilbite. Acta Crystallographica, B27, 833–841.

Galli, E. and Alberti, A. (1975a) The crystal structure of stellerite. Bulletin Société, Francaise de Minéralogie et du Cristallographie, 98, 11–18.

——— (1975b) The crystal structure of barrerite. Bulletin de la Société Francaise de Minéralogie et du Cristallographie, 98, 331–340.

Gottardi, G. and Galli, E. (1985) Natural zeolites, 409 p. Springer-Verlag, Berlin.

Hastings, J.B., Suortti, P., Thomlinson, W., Kvick, Å, and Koetzle, T.F. (1983) Optical design for the NSLS crystallographic beam line. Nuclear Instruments and Methods, 208, 55–58.

Howard, C.J. (1982) The approximation of asymmetric neutron powder diffraction peaks by sums of Gaussians. Journal of Applied Crystallography, 15, 615–620.

Larson, A.C. and Von Dreele, R.B. (1994) GSAS. General Structure Analysis System. Report LAUR 86–748, Los Alamos National Laboratory, Los Alamos, New Mexico.

Meier, W.M. and Olson, D.H. (1978) Atlas of Zeolite Structure Types. Juris Druck Verlag A.G., Zürich, Switzerland.

Mortier, W.J. (1983) Thermal stability of the stilbite-type framework: crystal structure of the dehydrated sodium/ammonium exchange form. American Mineralogist, 68, 414–419.

Parise, J.B., Corbin, D.R., Abrams, L., and Cox, D.E. (1984) Structure of dealuminated LindeY-zeolite; $Si_{139.7}Al_{52.3}O_{384}$ and $Si_{173.1}Al_{18.9}O_{384}$: presence of non-framework Al species. Acta Crystallographica, C40, 1493–1497.

Pearce, J.R., Mortier W.J., King G.S.D., Pluth, J.J., Steele, I.M., and Smith J.V. (1980) Stabilization of the stilbite-type framework: crystal structure of the dehydrated $NH_4$-exchanged form. In L.V.C. Rees, Ed., Proceedings of the Fifth International Conference on Zeolites, p. 261. Naples, Heyden, London.

Quartieri, S. and Vezzalini, G. (1987) Crystal chemistry of stilbites: structure refinements of one normal and four chemically anomalous samples. Zeolites, 7, 163–170.

Simonot-Grange, M.H., Cointot, A., and Thrierr-Sorel, A. (1970) Etude des systémes divariants zéolite-eau. Cas de la stilbite. Comparaison avec la heulandite. Bulletin de la Société Chimique de France 12, 4286–4297. (in French)

Slaughter, M. (1970) Crystal structure of stilbite. American Mineralogist, 55, 387–397.

Ståhl, K. (1994) Real-time powder diffraction studies of zeolite dehydration processes. Material Science Forum, 166–169, 571–576.

Ståhl, K. and Hanson, J. (1995) Real-time X-ray synchrotron powder diffraction studies of the dehydration process in scolecite and mesolite. Journal of Applied Crystallography, 27, 543–550.

Ståhl, K. and Thomasson, R. (1992) Using CPS120 (Curved Position-Sensitive Detector Covering 120°) powder diffraction data in Rietveld analysis. The dehydration process in zeolite thomsonite. Journal of Applied Crystallography, 25, 251–258.

Thompson, P., Cox, D.E., and Hastings, J. B. (1987) Rietveld refinement of Debye-Scherrer synchrotron X-ray data for $Al_2O_3$. Journal of Applied Crystallography, 20, 79–83.

Ziebold, T.O. and Ogilvie, R.E. (1964) An empirical method for electron microanalysis. Analytical Chemistry, 36, 322–327.

Manuscript received August 6, 1996
Manuscript accepted March 4, 1997